

**Enhanced superconductivity in LaRu_3Si_2
by chemical pressure tuning of kagome flat bands**

Ryo Misawa¹, Markus Kriener², Rinsuke Yamada¹, Ryota Nakano¹,
Milena Jovanovic^{2,3}, Leslie M. Schoop², and Max Hirschberger^{1,4*}

¹*Department of Applied Physics and Quantum-Phase Electronics Center (QPEC),
The University of Tokyo, Bunkyo, Tokyo 113-8656, Japan*

²*Department of Chemistry, Princeton University,
Princeton 08540, New Jersey, USA*

³*Department of Chemistry, North Carolina State University,
Raleigh, 27695, North Carolina, USA and*

⁴*RIKEN Center for Emergent Matter Science (CEMS), Wako, Saitama 351-0198, Japan*

(Dated: March 31, 2025)

arXiv:2503.22477v1 [cond-mat.supr-con] 28 Mar 2025

*Electronic address: hirschberger@ap.t.u-tokyo.ac.jp

Abstract

In kagome metals, flat bands induced by frustrated hopping serve as a platform for strong electronic correlation, while often exhibiting substantial dispersion along the k_z direction due to interlayer coupling. Here, we investigate the superconductivity of kagome metal $\text{LaRu}_3(\text{Si}_{1-x}\text{Ge}_x)_2$ by chemical pressure tuning while preserving the Ru-4*d* states that constitute the kagome flat bands. We observe a sizable enhancement in the density of states up to $x = 0.07$, as determined by the specific heat, with a concomitant increase in the superconducting transition temperature. As supported by our first-principles calculations, the lattice expansion along the c -axis by chemical pressure mitigates a detrimental effect of hybridization between kagome layers, thereby reinforcing the three-dimensional localization of flat-band electrons. Providing evidence for LaRu_3Si_2 as a flat-band hosting superconductor, we demonstrate a simple, yet effective, route to engineer flat bands by uniaxial lattice expansion.

Main Text

The kagome lattice, a two-dimensional network of corner-sharing triangles, features three sublattice degrees of freedom per unit cell. Kagome metals serve as a platform for investigating the intricate interplay between electron-electron correlations and the topology of electronic band structures. [1–3]. This study discusses superconductivity in the intermetallic LaRu_3Si_2 , where the kagome lattice is formed by Ru atoms as depicted in Fig. 1(a). Considering first a single orbital model on an isolated kagome lattice in Fig. 1(b), one obtains three bands forming a flat band and Dirac cone, and with van-Hove singularities at the M -points in the Brillouin zone [Fig. 1(c)]. In particular, the dispersionless upper band originates from frustrated hopping between the three sites of the kagome lattice [4]. Further introducing Kane-Mele type spin-orbit coupling [5], a gap opens between the Dirac cone and the flat band, imparting a Chern number onto the flat band in this two-dimensional model [6–8].

Real-world kagome metals retain the features of this simplified electronic structure if the coupling between consecutive kagome layers is weak, and mostly 3*d* electron systems have been considered as realizations of this scenario [8–13]. As an example, Fig. 1(d) presents the electronic band structure of LaRu_3Si_2 , which hosts an hourglass-shaped dispersion originating from Ru-4*d* orbitals along the Γ - K - M path. Early experimental work and a recent

theoretical study emphasize that LaRu_3Si_2 distinguishes itself as the only known kagome superconductor hosting flat bands near the Fermi level without magnetic order [14, 15]. It is further suggested that the flat bands may be a driver of superconductivity with the highest observed transition temperature $T_c = 6.7\text{ K}$ among the family of RT_3M_2 ($R = \text{rare-earth}$, $T = \text{transition metal}$ and $M = \text{main group element}$) [14, 16–21] and among Kagome metals as a material class [22]. Moreover, charge-density-wave orders, possibly accompanied by breaking of time-reversal symmetry, have been recently observed [23, 24], reminiscent of the kagome superconductors $AV_3\text{Sb}_5$ ($A = \text{K, Cs, and Rb}$) [25, 26].

Real kagome metals are three-dimensional, and their flat bands often exhibit strong dispersion along the k_z direction of reciprocal space [8, 13, 27]. This behavior is also observed in LaRu_3Si_2 along the $\Gamma - A$ line in Fig. 1(d). Therefore, flat-band electrons are not fully localized in known bulk kagome metals. To achieve tailored flat bands, it has thus been proposed to either suppress interlayer coupling [t_{out} in Fig. 1 (b)] by isolating kagome layers [28], or to introduce 3D frustrated hopping [29]. For the latter approach, 3D flat bands have been predicted for the pyrochlore lattice [30], a 3D analogue of the kagome lattice, and have recently been observed [29, 31]. Despite its simplicity, the former approach has not yet been conclusively implemented to enhance electron correlation phenomena and superconductivity on the kagome lattice.

Here, we engineer the electronic structure of LaRu_3Si_2 by substituting Si with the larger volume element Ge. We observe a marked increase of the superconducting critical temperature T_c . An enhancement of the total density of states (DOS) with Ge-doping underpins the observed evolution of T_c , as confirmed by specific heat measurements. Our electronic structure calculations demonstrate that anisotropic lattice expansion along the c -axis isolates the kagome layers, weakens the interlayer hopping t_{out} , and promotes the DOS at the Fermi level while keeping the intralayer hopping t intact. As summarized in Fig. 1(e), this is in stark contrast to previous attempts to tune superconductivity in LaRu_3Si_2 by chemical substitution at the Ru site, which generally results in a sharp decrease of T_c [32–34].

Crystals were obtained by the melting technique [35]. In Fig. 2(a), the LaRu_3Si_2 structure was confirmed by powder X-ray diffraction (XRD). The absence of the LaRu_2Si_2 phase is confirmed. Figure 2(c,d) shows the hexagonal lattice constants of $\text{LaRu}_3(\text{Si}_{1-x}\text{Ge}_x)_2$ (LRSG) extracted from XRD and their evolution with x based on the LeBail analysis in the $P6/mmm$ structure. This neglects minor effects of symmetry-lowering charge order in this family of

compounds [23]. We find a robust value of a and a linear expansion of the out-of-plane lattice constant c , which in combination gives a linear volume expansion in Fig. 2(e). The latter is consistent with Vegard's law, and in good agreement with the trend derived from structure relaxation calculations of LaRu_3Si_2 and LaRu_3Ge_2 . Magnetization and specific heat measurements were performed in a commercial cryostat [35].

To confirm the bulk superconducting state in LRSG, we show the magnetic susceptibility χ in Fig. 3(a). Above the transition temperature T_c , χ is small and positive, consistent with the weak paramagnetic Pauli susceptibility of LaRu_3Si_2 [36]. Strong diamagnetism accompanying the superconducting transition appears as a sharp drop in the data around $6 \sim 7$ K.

To precisely determine T_c , we measure the specific heat $C(T)$ in zero field and at 5 T, which is high enough to entirely suppress the superconductivity [Fig. 3(b)]. In the former traces, a sharp kink appears at T_c , the second-order transition into the superconducting state. We model the normal state contribution C_N by electronic and phonon terms, viz. $C_N(T) = \gamma T + \beta T^3 + \eta T^5$ [lines in Fig. 3(b)]. The higher order phonon contribution ηT^5 is necessary to describe the data [37]. After subtraction of $C_N(T)$, we fit the superconducting specific heat $C(T) - C_N(T)$ to the prediction of Bardeen-Cooper-Schrieffer (BCS) theory by equal-area construction in Fig. 3(c) [38], confirming an enhancement in T_c with x . Next, we discuss the evolution of γ and β from the fit of $C_N(T)$ in Fig. 3(d). A clear increase of γ and β is observed with x . Given the formula $\gamma = \pi^2 k_B^2 N(E_F)/3$ with $N(E_F)$ being the density of states at the Fermi energy E_F , the enhancement of γ corresponds to an increase of $N(E_F)$ [Fig. 3(e)]. The trend is reproduced by DFT, where $N(E_F)$ increases from 2.9 states/eV/u.c/spin to 3.3 states/eV/u.c/spin as seen in Fig. 3(f). The marked enhancement of $N(E_F)$ goes hand in hand with an increase of T_c , reaching up to 7.1 K for $x = 0.07$ [Fig. 3(e)].

The increase of $N(E_F)$ and T_c qualitatively follows the McMillan equation

$$T_c = \frac{\Theta_D}{1.45} \exp\left(\frac{-1.04(1 + \lambda)}{\lambda - \mu^*(1 + 0.62\lambda)}\right), \quad (1)$$

where Θ_D is the Debye temperature, λ is the electron-phonon coupling constant, and μ^* is the Coulomb pseudopotential, which usually takes a value around 0.1 for a metal [39]. Assuming a relatively static pairing potential V , the enhancement of $N(E_F)$ directly corresponds to that of λ , as given by the relation $N(E_F)V = (\lambda - \mu^*)/(1 + \lambda)$, which in turn promotes

T_c [35].

The observed enhancement of γ can be attributed to the expansion of the lattice constant c , as illustrated in Fig. 3(e). This interpretation is further supported by our band structure calculations for LaRu_3Ge_2 . The projected band structures for LaRu_3Ge_2 and LaRu_3Si_2 are shown in Fig. 4(a),(b). Focusing on the $\Gamma - A$ line, which is parallel to the k_z -axis, we find that substitution of Si with Ge decreases the bandwidth of flat bands at E_F . This indicates that the uniaxial lattice expansion along the c -axis by Ge doping suppresses interlayer coupling between kagome layers. Furthermore, the partial density of states in Fig. 4(c),(d) reveals a preference for the planar $4d_{xy}$ orbital over $4d_{z^2}$, with the latter exhibiting stronger hybridization along the z -direction. We note that the partial density of states (PDOS) for Ru- $4d_{xz}$ around E_F is hardly affected by Ge substitution [35]. Importantly, Ge substitution leaves the crucial kagome lattice plane of Ru atoms mostly undisturbed, providing a powerful route for tuning superconductivity in LaRu_3Si_2 . We stress the general applicability of such careful alloying studies to binary and ternary kagome metals [40], with wide tunability of electronic properties, charge ordering, and superconductivity.

Acknowledgements We thank T.-h. Arima for enlightening discussions. This work was supported by JSPS KAKENHI Grants Nos. JP21K13877, JP22H04463, JP22K20348, JP23H05431, 23K13057, 24H01607, and 24H01604, as well as JST CREST Grant Nos. JPMJCR1874 and JPMJCR20T1 (Japan) and JST FOREST Grant No. JPMJFR2238 (Japan). This work was supported by Japan Science and Technology Agency (JST) as part of Adopting Sustainable Partnerships for Innovative Research Ecosystem (ASPIRE), Grant Number JPMJAP2426. Work at Princeton was supported by NSF, grant OAC-2118310, and by NSF through the Princeton Center for Complex Materials, a Materials Research Science and Engineering Center DMR-2011750.

-
- [1] J. Yin, B. Lian, and M. Z. Hasan, *Nature* **612**, 647 (2022).
 - [2] Y. Wang, H. Wu, G. T. McCandless, J. Y. Chan, and M. N. Ali, *Nat. Rev. Phys.* **5**, 635 (2023).
 - [3] J. G. Checkelsky, B. A. Bernevig, P. Coleman, Q. Si, and S. Paschen, *Nat. Rev. Mater.* **9**, 509

- (2024).
- [4] D. L. Bergman, C. Wu, and L. Balents, *Phys. Rev. B Condens. Matter Mater. Phys.* **78**, 125104 (2008).
 - [5] C. L. Kane and E. J. Mele, *Phys. Rev. Lett.* **95**, 146802 (2005).
 - [6] H. Guo and M. Franz, *Phys. Rev. B Condens. Matter* **80**, 113102 (2009).
 - [7] A. Bolens and N. Nagaosa, *Phys. Rev. B Condens. Matter* **99**, 165141 (2019).
 - [8] M. Kang, S. Fang, L. Ye, H. C. Po, J. Denlinger, C. Jozwiak, A. Bostwick, E. Rotenberg, E. Kaxiras, J. G. Checkelsky, et al., *Nat. Commun.* **11**, 4004 (2020).
 - [9] Z. Lin, J. Choi, Q. Zhang, W. Qin, S. Yi, P. Wang, L. Li, Y. Wang, H. Zhang, Z. Sun, et al., *Phys. Rev. Lett.* **121**, 096401 (2018).
 - [10] M. Kang, L. Ye, S. Fang, J. You, A. Levitan, M. Han, J. I. Facio, C. Jozwiak, A. Bostwick, E. Rotenberg, et al., *Nat. Mater.* **19**, 163 (2019).
 - [11] M. Li, Q. Wang, G. Wang, Z. Yuan, W. Song, R. Lou, Z. Liu, Y. Huang, Z. Liu, H. Lei, et al., *Nat. Commun.* **12**, 1 (2021).
 - [12] N. Regnault, Y. Xu, M. Li, D. Ma, M. Jovanovic, A. Yazdani, S. S. P. Parkin, C. Felser, L. M. Schoop, N. P. Ong, et al., *Nature* **603**, 824 (2022).
 - [13] L. Ye, S. Fang, M. Kang, J. Kaufmann, Y. Lee, C. John, P. M. Neves, S. Y. F. Zhao, J. Denlinger, C. Jozwiak, et al., *Nat. Phys.* **20**, 610 (2024).
 - [14] C. Mielke, Y. Qin, J. Yin, H. Nakamura, D. Das, K. Guo, R. Khasanov, J. Chang, Z. Q. Wang, S. Jia, et al., *Phys. Rev. Mater.* **5**, 034803 (2021).
 - [15] D. Junze, J. Yi, T. F. T. Cerqueira, H. Haoyu, O. L. Eeli, C. Dumitru, P. Hanqi, W. Zhijun, G. V. Maia, M. Emilia, et al., arXiv:2503.20867 [cond-mat.supr-con] (2025).
 - [16] H. Barz, *Mater. Res. Bull.* **15**, 1489 (1980).
 - [17] H. C. Ku, G. P. Meisner, F. Acker, and D. C. Johnston, *Solid State Commun.* **35**, 91 (1980).
 - [18] S. Chaudhary, Shama, J. Singh, A. Consiglio, D. D. Sante, R. Thomale, and Y. Singh, *Phys. Rev. B.* **107**, 085103 (2023).
 - [19] X. Gui and R. J. Cava, *Chem. Mater.* **34**, 2824 (2022).
 - [20] U. Rauchschwalbe, W. Lieke, F. Steglich, C. Godart, L. C. Gupta, and R. D. Parks, *Phys. Rev. B Condens. Matter* **30**, 444 (1984).
 - [21] C. Gong, S. Tian, Z. Tu, Q. Yin, Y. Fu, R. Luo, and H. Lei, *Chin. Physics Lett.* **39**, 087401 (2022).

- [22] J. Deng, Y. Jiang, T. F. T. Cerqueira, H. Hu, E. O. Lamponen, D. Călugăru, Z. W. Hanqi Pi, M. G. Vergniory, E. Morosan, T. Neupert, et al., arXiv:2503.20867 (2025).
- [23] I. Plokhikh, C. Mielke, H. Nakamura, V. Petricek, Y. Qin, V. Sazgari, J. Küspert, I. Bialo, S. Shin, O. Ivashko, et al., Commun. Phys. **7**, 1 (2024).
- [24] C. Mielke, V. Sazgari, I. Plokhikh, S. Shin, H. Nakamura, J. N. Graham, J. Küspert, I. Bialo, G. Garbarino, D. Das, et al., arXiv:2402.16219 [cond-mat.supr-con] (2024).
- [25] S. D. Wilson and B. R. Ortiz, Nat. Rev. Mater. **9**, 420 (2024).
- [26] B. R. Ortiz, L. C. Gomes, J. R. Morey, M. Winiarski, M. Bordelon, J. S. Mangum, I. W. H. Oswald, J. A. Rodriguez-Rivera, J. R. Neilson, S. D. Wilson, et al., Phys. Rev. Mater. **3**, 094407 (2019).
- [27] H. Huang, L. Zheng, Z. Lin, X. Guo, S. Wang, S. Zhang, C. Zhang, Z. Sun, Z. Wang, H. Weng, et al., Phys. Rev. Lett. **128**, 096601 (2022).
- [28] M. Jovanovic and L. M. Schoop, J. Am. Chem. Soc. **144**, 10978 (2022).
- [29] J. P. Wakefield, M. Kang, P. M. Neves, D. Oh, S. Fang, R. McTigue, S. Y. F. Zhao, T. N. Lamichhane, A. Chen, S. Lee, et al., Nature **623**, 301 (2023).
- [30] H. Guo and M. Franz, Phys. Rev. Lett. **103**, 206805 (2009).
- [31] J. Huang, L. Chen, Y. Huang, C. Setty, B. Gao, Y. Shi, Z. Liu, Y. Zhang, T. Yilmaz, E. Vescovo, et al., Nat. Phys. **20**, 603 (2024).
- [32] S. Li, J. Tao, X. Wan, X. Ding, H. Yang, and H. Wen, Phys. Rev. B Condens. Matter **86**, 024513 (2012).
- [33] B. Li, S. Li, and H. Wen, Phys. Rev. B Condens. Matter **94**, 094523 (2016).
- [34] S. Chakraborty, R. Kumar, and N. Mohapatra, Phys. Rev. B Condens. Matter **107**, 024503 (2023).
- [35] See Supplementary Information at (URL to be inserted by publisher).
- [36] Y. Kishimoto, T. Ohno, T. Hihara, K. Sumiyama, G. Ghosh, and L. C. Gupta, J. Phys. Soc. Jpn. **71**, 2035 (2002).
- [37] S. Li, B. Zeng, X. Wan, J. Tao, F. Han, H. Yang, Z. Wang, and H. Wen, Phys. Rev. B Condens. Matter **84**, 214527 (2011).
- [38] M. Tinkham, *Introduction to superconductivity: Second edition* (Courier Corporation, 2004).
- [39] J. P. Carbotte, Rev. Mod. Phys. **62**, 1027 (1990).
- [40] C. Chen, J. Zheng, Y. He, X. Ying, S. Sankar, L. Li, Y. Wei, X. Dai, H. C. Po, and B. Jäck,

- arXiv:2409.06933 [cond-mat.str-el] (2024).
- [41] Different reports in the literature show slightly different values of T_c of pure LaRu_3Si_2 . We shift the $T_c(x)$ so that $T_c(0)$ becomes 6.6 K.
- [42] P. Blaha, K. Schwarz, F. Tran, R. Laskowski, G. K. H. Madsen, and L. D. Marks, *J. Chem. Phys.* **152**, 074101 (2020).
- [43] J. P. Perdew, K. Burke, and M. Ernzerhof, *Phys. Rev. Lett.* **77**, 3865 (1996).
- [44] J. M. Vandenberg and H. Barz, *Mater. Res. Bull.* **15**, 1493 (1980).
- [45] W. Reese and W. L. Johnson, *Phys. Rev.* **2**, 2972 (1970).
- [46] M. Kriener, M. S. Bahramy, Y. Tokura, and Y. Taguchi, *Phys. Rev. B.* **106**, 134519 (2022).

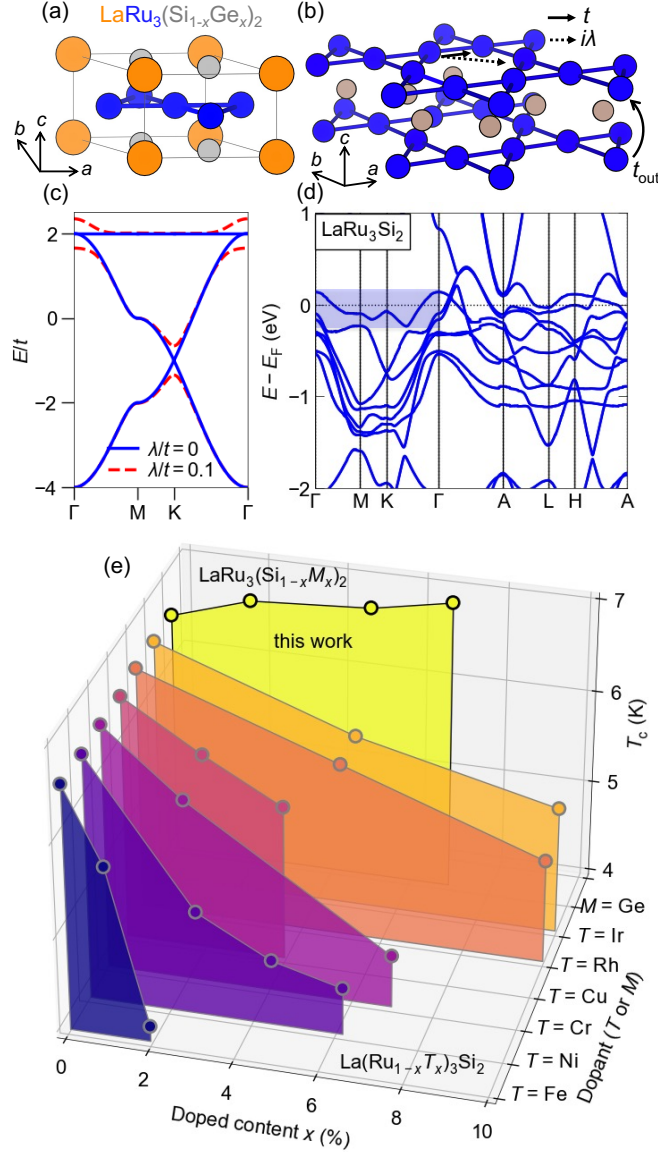


FIG. 1: (color online). Superconducting kagome metal $\text{LaRu}_3(\text{Si}_{1-x}\text{Ge}_x)_2$ (LRSG) with flat bands at the Fermi level. (a) Hexagonal structure of superconducting kagome metal LRSG. (b) The kagome motif of Ru atoms with Si and Ge between Ru layers. t and λ are the nearest-neighbor hopping and spin-orbit coupling, respectively. Uniaxial lattice expansion along c -axis suppresses out-of-plane hopping t_{out} . (c) Band dispersion of a single-orbital model on the kagome lattice, with Dirac cone and flat band (blue). The introduction of spin-orbit coupling opens a gap between the Dirac cone and the flat band (red). (d) Band structure of LaRu_3Si_2 . Blue shading highlights flat bands in the $k_x - k_y$ plane. (e) Superconducting transition temperature T_c for alloyed LaRu_3Si_2 [41]. This work demonstrates the enhancement of T_c by chemical pressure tuning, in contrast to previous attempts of band-filling tuning.

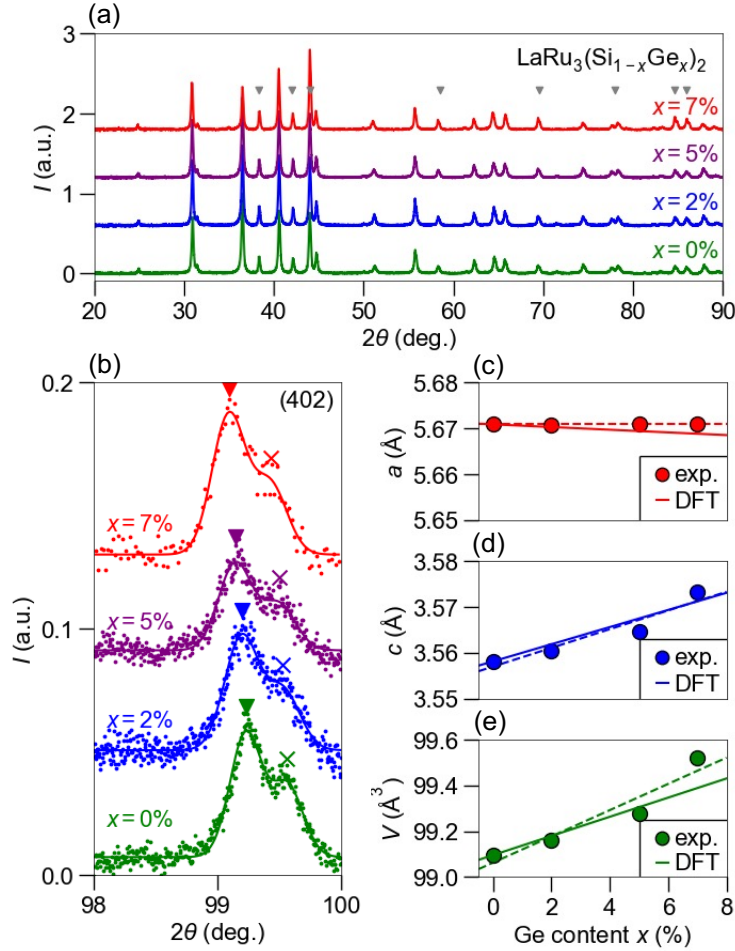


FIG. 2: (color online). Structural evolution of LaRu₃(Si_{1-x}Ge_x)₂ (LRSG). (a) Powder X-ray diffraction (XRD) pattern for four compositions of LRSG with normalized intensity. Impurity lines from excess Ru metal are indicated by grey triangles. (b) Systematic shift of (402) reflection as a function of x , measured using X-rays from Cu-K α_1 (triangle) and Cu-K α_2 (cross). The lines indicate a double-Gaussian fit to the data. Offsets are applied to each compound for clarity in panels (a,b). (c-e) Evolution of lattice constants a , c , and unit cell volume V for LRSG from LeBail analysis of the powder XRD (filled circle) and DFT calculations (solid line) in the approximate hexagonal structure. Dotted lines correspond to linear fits to the data. Solid lines are derived from structure optimization by the DFT calculations for LaRu₃Si₂ and LaRu₃Ge₂. A constant offset is applied to the DFT data to align with the experimental values at $x = 0$.

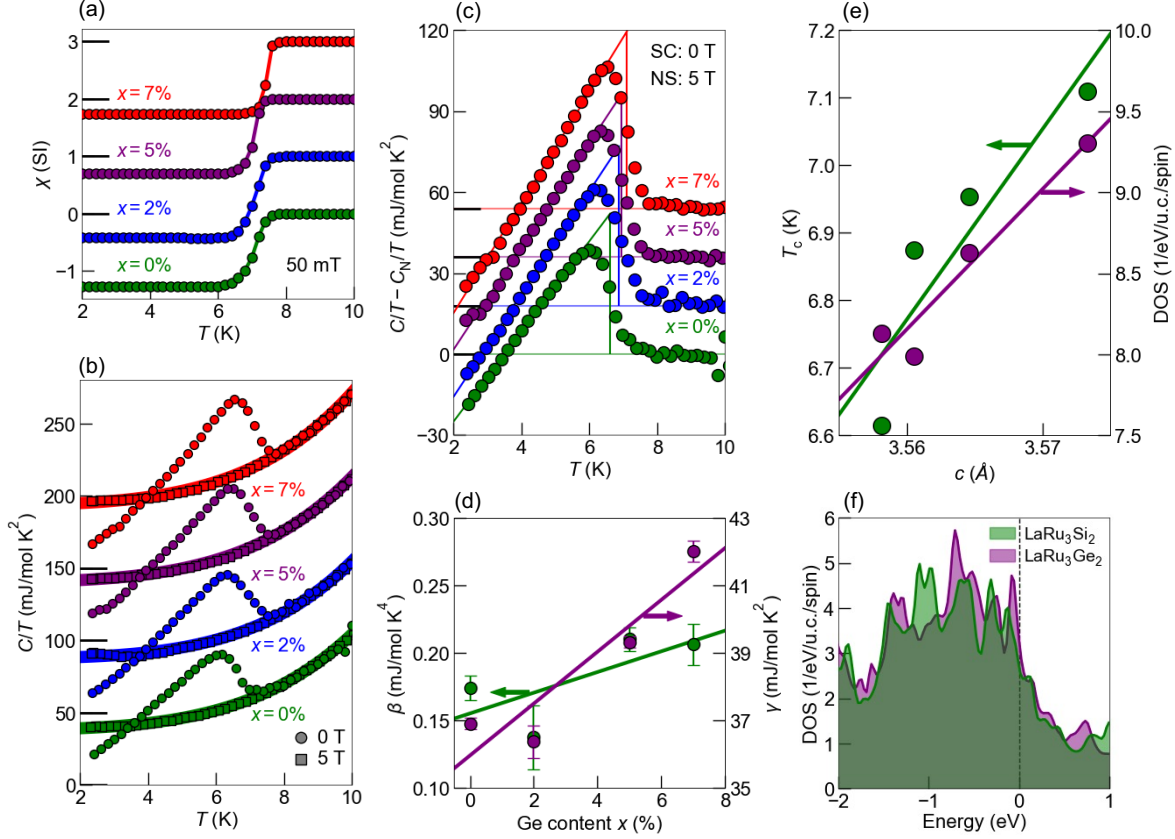


FIG. 3: (color online). Enhancement of superconductivity by chemical pressure tuning in $\text{LaRu}_3(\text{Si}_{1-x}\text{Ge}_x)_2$ (LRSG). (a) Magnetic susceptibility $\chi = M/H$ in the SI unit. The onset of a rapid drop indicates the Meissner effect of a bulk superconducting state; demagnetization correction was applied [35]. (b) Specific heat $C(T)$ in zero magnetic field (round symbols) and in a field large enough to suppress the superconducting state (square symbols). Lines are a fit to the normal state specific heat $C_N(T)$ using $C_N(T) = \gamma T + \beta T^3 + \eta T^5$. (c) After subtraction of $C_N(T)$, we perform a linear fit for $C(T) - C_N(T)$ by equal-area construction (solid lines). Offsets are applied to each dataset for clarity, with the zero values marked by bold ticks in panels (a-c). (d) Evolution of fit parameters extracted from $C_N(T)$ as a function of Ge content x . (e) Superconducting transition temperature T_c and DOS calculated from γ as a function of hexagonal lattice constant c . (f) Density of states (DOS) from density functional theory for LaRu_3Si_2 and (hypothetical) LaRu_3Ge_2 . The DOS at the Fermi level is 2.9 states/eV/u.c./spin and 3.3 states/eV/u.c./spin for LaRu_3Si_2 and LaRu_3Ge_2 , respectively.

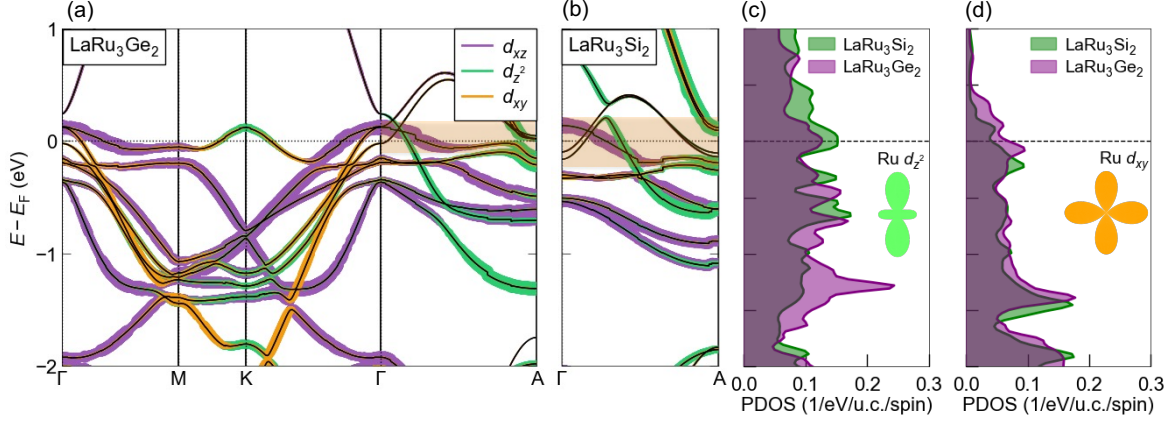


FIG. 4: (color online). Electronic structure of LaRu₃Ge₂ in comparison with LaRu₃Si₂. (a) Projected band structure of LaRu₃Ge₂ in the $k_x - k_y$ plane and along the $\Gamma - A$ line. Bands that are flat in the $k_x - k_y$ plane are highlighted in orange along the path parallel to the k_z -axis. (b) Projected band structure of LaRu₃Si₂ along the $\Gamma - A$ line. Bandwidth of the flat bands along this path is wider for LaRu₃Si₂. (c, d) Partial density of states (PDOS) for Ru-4 d_{z^2} and Ru-4 d_{xy} states of LaRu₃Si₂ and LaRu₃Ge₂. The contributions of Ru-4 d_{z^2} and Ru-4 d_{xy} at E_F are shown to be suppressed and enhanced by replacing Si with Ge, respectively. The PDOS for Ru-4 d_{xz} remains unchanged at the Fermi level as shown in Supplementary Information [35].

Supplementary Information

S I. DENSITY FUNCTIONAL CALCULATION

First-principles calculations are carried out using the WIEN2k software package, which employs the full-potential linearized augmented plane wave (FP-LAPW) method with local orbitals [42]. The exchange-correlation energy is treated within the Generalized Gradient Approximation (GGA) using the functional formulated by Perdew, Burke, and Ernzerhof (PBE) [43] in the $P6/mmm$ structure. We employ a uniform grid of 4096 k -points to ensure accurate sampling of the Brillouin zone and relax the lattice constants a and c . This yields $a = 5.8260\text{\AA}$, $c = 3.5666\text{\AA}$ for LaRu_3Si_2 and $a = 5.7967\text{\AA}$, $c = 3.7538\text{\AA}$ for hypothetical LaRu_3Ge_2 . We calculate the band structures and the density of states in the presence of spin-orbit coupling. For the density of states (DOS) and partial density of states (PDOS), we divide the calculated values by 2 to express them in units of eV^{-1} per unit cell (u.c.) per spin.

Fig. S1 shows our PDOS for the Ru- $4d_{z^2}$, Ru- $4d_{xy}$, and Ru- $4d_{xz}$ states of LaRu_3Si_2 and LaRu_3Ge_2 . The symmetrically equivalent Ru- $4d_{x^2-y^2}$ and Ru- $4d_{yz}$ states are not shown separately. We provide projected band structures in the full Brillouin zone for LaRu_3Si_2 and LaRu_3Ge_2 in Fig. S2.

S II. CRYSTAL GROWTH

Crystals of $\text{LaRu}_3(\text{Si}_{1-x}\text{Ge}_x)_2$ (LRSG) are prepared by arc melting in argon atmosphere after careful evacuation to 10^{-3} Pa. The ingot is turned and remelted at least three times, and weight loss is typically around 0.5%. To stabilize the LaRu_3Si_2 structure over the competing phase LaRu_2Si_2 , excess Ru metal is added to the starting composition [14, 16, 36, 37, 44]. The solution limit of Ge is found to be $x = 0.07$, and the required amount of Ru increases when approaching this value: We use a melt of starting composition $\text{LaRu}_{4.5}(\text{Si}_{1-x}\text{Ge}_x)_2$ for $x = 0, 0.02, 0.05$, and $\text{LaRu}_5(\text{Si}_{1-x}\text{Ge}_x)_2$ for $x = 0.07$.

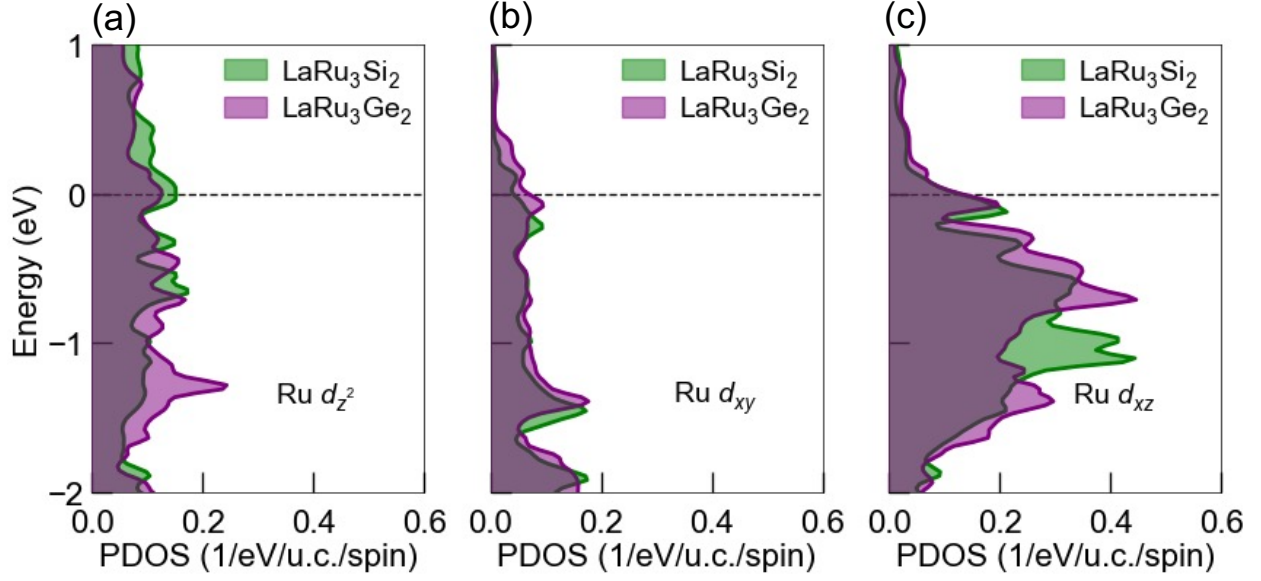


FIG. S1: (color online). Partial density of states (PDOS) for Ru- $4d_{z^2}$, Ru- $4d_{xy}$, and Ru- $4d_{xz}$ states of LaRu_3Si_2 and LaRu_3Ge_2 .

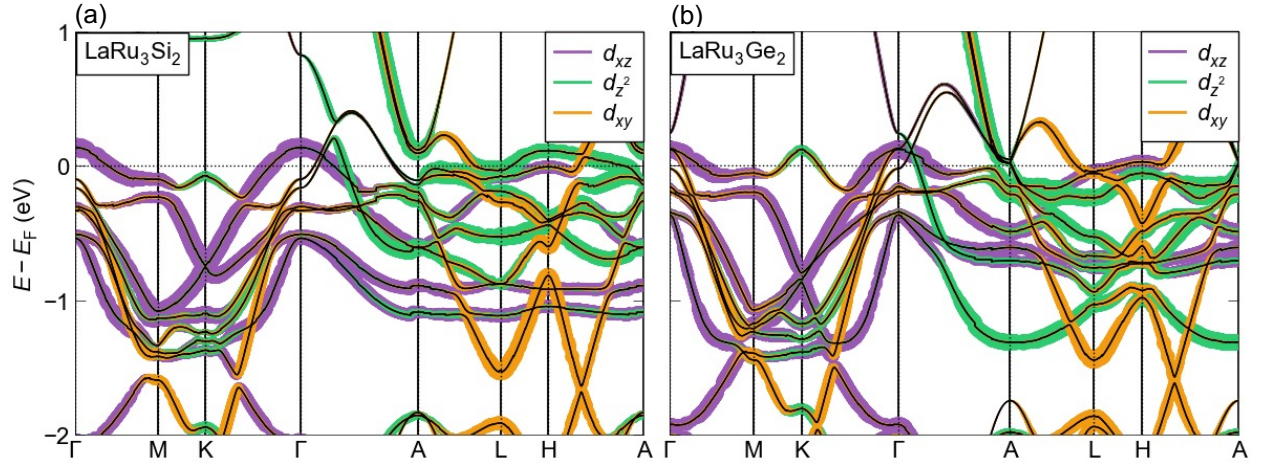


FIG. S2: (color online). Projected band structure of LaRu_3Si_2 (a) and LaRu_3Ge_2 (b) in the full Brillouin zone.

S III. POWDER X-RAY DIFFRACTION

We perform powder X-ray diffraction (XRD) to confirm the formation of $\text{LaRu}_3(\text{Si}_{1-x}\text{Ge}_x)_2$ as well as the absence of the competing LaRu_2Si_2 (122). The data include reflections from nonmagnetic, elemental Ru, because Ru was added to the melt to destabi-

lize the chemically stable 122 phase. In the main text, we neglect minor effects of subtle orthorhombic distortions in this compound. This approximation is justified by the Rietveld analysis, as the major reflections are well accounted for by space group $P6/mmm$.

S IV. MAGNETIC SUSCEPTIBILITY MEASUREMENT

We perform magnetization measurements to detect the superconducting Meissner effect in a low magnetic field of $\mu_0 H = 0.05$ T. Samples of mass ~ 100 mg were mounted in a Quantum Design Magnetic Properties Measurement System (MPMS). We correct for the demagnetization effect in χ by approximating our roughly shaped crystals as a sphere, which has a demagnetization factor $N = 1/3$. The intrinsic susceptibility is then obtained using the relation: $\chi = \chi_{\text{exp}}/(1 - N\chi_{\text{exp}})$. Slightly smaller values than the ideal $\chi = -1$ (perfect Meissner shielding) may arise due to deviations from the spherical approximation.

S V. SPECIFIC HEAT MEASUREMENT

We measure specific heat by the relaxation technique in a Quantum Design Physical Properties Measurement System (PPMS). For each measurement, the addenda (with Apiezon N grease mounted on the stage) are measured before setting the sample for the main measurement. To eliminate contributions from non-magnetic impurity Ru metal, we subtract $\gamma_{\text{Ru}} = 2.8$ mJ/molK² and $\beta_{\text{Ru}} = 0.068$ mJ/molK⁴ from the total γ and β values [37, 45]. For each value, we multiply the ratio of Ru impurity $y/3$, where y represents the ratio of excess Ru, namely $y = 1.5$ for $x = 0, 0.02, 0.05$ and $y = 2$ for $x = 0.07$. We summarize γ and β values before and after the subtraction of the Ru contribution in Table I. Errors for the fitting parameters β and γ in Fig. 3(d) are estimated by the bootstrap method. We estimate the density of states (DOS) at the Fermi energy, $N(E_{\text{F}})$, using the relation

$$N(E_{\text{F}}) = \frac{3\gamma}{\pi^2 k_{\text{B}}^2}, \quad (\text{S1})$$

which has units of J⁻¹. We convert this to eV⁻¹ per unit cell (u.c.). Furthermore, since γ is calculated assuming a spinless electronic structure, we divide by 2 to obtain $N(E_{\text{F}})$ in units of eV⁻¹ per unit cell per spin [38, 46].

For the superconducting state, the specific heat can be fitted by an analytical expression within the framework of the BCS theory. Here we approximate the temperature dependence

to be linear below T_c , which is valid for our temperature range (> 2 K) [19]. This method allows us to precisely determine T_c by the equal-area construction, which is crucial for tracking the evolution of T_c in our crystals: We first numerically calculate the area under the curve of $\Delta C/T = C/T - C_N/T$ below 8 K, denoted as S [Fig. S3(a)]. We then fit $\Delta C/T$ below 6 K by a linear function $\Delta C/T = aT + b$. Imposing entropy conservation, the area under the curve is thus given by

$$S = \frac{1}{2}(T_c - T_0)(aT_c + b) - \frac{1}{2}(T_0 - T_{\min})|aT_{\min} + b|, \quad (\text{S2})$$

where $T_0 = -b/a$ is the intercept of the linear fit, and T_{\min} is the lowest temperature at which data were taken. The first term corresponds to the area for $T_0 \leq T \leq T_c$ and the second to that for $T_{\min} \leq T \leq T_c$, as illustrated in Fig. S3(b). Solving this equation, we analytically determine the transition temperature as

$$T_c = \frac{-b + \sqrt{b^2 + 2aS + a^2T_{\min}^2 + 2abT_{\min}}}{a}. \quad (\text{S3})$$

Furthermore, we obtain the specific heat jump at T_c as

$$\Delta C(T_c)/T_c = aT_c + b. \quad (\text{S4})$$

We provide the calculated ratio $\Delta C(T_c)/\gamma T_c$ in Table I. A slight deviation from the BCS value of 1.43 may suggest a moderate superconducting coupling strength. Given that the Sommerfeld coefficient of pure Ru is small ($\gamma_{\text{Ru}} = 2.8$ mJ/mol K²), the residual specific heat contribution from the Ru impurity is expected to be negligible.

To explore the effects of β and γ on T_c , we consider the McMillan equation

$$T_c = \frac{\Theta_D}{1.45} \exp\left(\frac{-1.04(1 + \lambda)}{\lambda - \mu^*(1 + 0.62\lambda)}\right), \quad (\text{S5})$$

where Θ_D is the Debye temperature, λ is the electron-phonon coupling constant, and μ^* is the Coulomb pseudopotential [39]. The electron-phonon coupling λ is expressed in terms of the density of states at the Fermi level, $N(E_F)$, as

$$N(E_F)V = \frac{\lambda - \mu^*}{1 + \lambda} \quad (\text{S6})$$

$$= 1 - \frac{1 + \mu^*}{1 + \lambda}, \quad (\text{S7})$$

where V denotes the pairing potential. This relation indicates that an increase in γ will also enhance λ , thereby promoting T_c ; this is assuming a relatively static value of V . Meanwhile,

the Debye temperature Θ_D is related to β viz.

$$\Theta_D = \left(\frac{12\pi^4 N k_B}{5\beta} \right)^{\frac{1}{3}}, \quad (\text{S8})$$

where N is the number of atoms per formula unit. Since Θ_D scales inversely with $\beta^{1/3}$, an increase in β suppresses Θ_D , leading to a reduction in T_c . Overall, while both β and γ influence T_c , the observed enhancement of T_c suggests that the effect of γ dominates. Setting $\mu^* = 0.13$, we estimate λ to be $0.63 \sim 0.66$ from Eq. (S5), as summarized in Table I. The enhanced electron-phonon coupling constant $\lambda > 0.5$ suggests a moderately coupled superconductor. This is consistent with $\Delta C(T_c)/\gamma T_c > 1.43$.

With λ determined, we compute the bare density of states, $N_{\text{bare}}(E_F)$, using

$$N_{\text{bare}}(E_F) = \frac{N(E_F)}{1 + \lambda}, \quad (\text{S9})$$

which allows for comparison to band structure calculations. This yields approximately $N_{\text{bare}}(E_F) = 51/\text{eV}/\text{u.c}/\text{spin}$ and reasonably corresponds to the calculated DOS at $E = -0.1 \text{ eV}$ in Fig. 3(f).

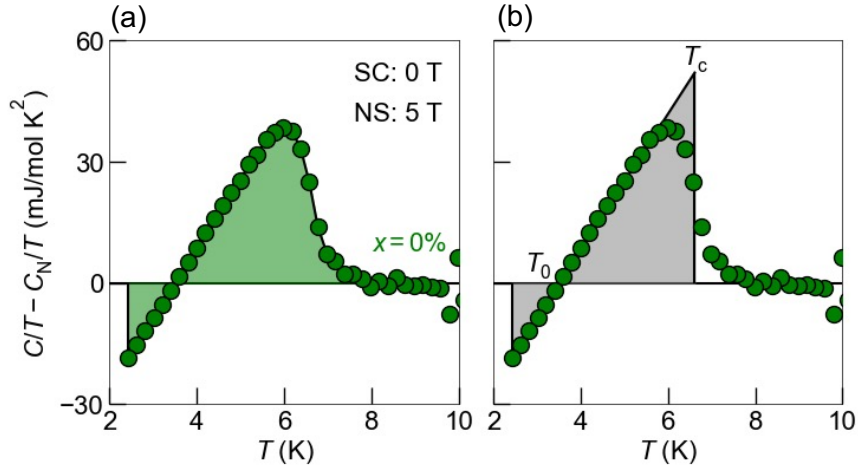


FIG. S3: (color online). Fitting of superconducting specific heat $\Delta C = C - C_N$ and equal-area construction. As a representative example, we show the procedure for LaRu_3Si_2 . (a) The area under the curve (green) is calculated numerically. (b) $\Delta C/T$ is fitted by a linear approximation of the BCS expression. T_c is identified such that the gray areas equal the green area in panel (a). T_0 denotes the intercept of the fit.

TABLE I: Properties of $\text{LaRu}_3(\text{Si}_{1-x}\text{Ge}_x)_2$ probed by specific heat measurements. For the electron and phonon contributions γ and β , values before and after subtracting a subtle contribution from Ru impurity in $\text{LaRu}_3(\text{Si}_{1-x}\text{Ge}_x)_2 + y\text{Ru}$ are given. $\Delta C(T_c)$ denotes the specific heat jump at T_c , and $\Delta C(T_c)/\gamma T_c = 1.43$ holds for weakly coupled superconductors. $N(E_F)$ and λ denote the DOS and the electron-phonon coupling constant, respectively.

Ge content x	0	0.02	0.05	0.07
γ (mJ/molK ²)	38.3	37.4	40.7	43.8
$\gamma - y/3 \cdot \gamma_{\text{Ru}}$ (mJ/molK ²)	36.9	36.0	39.3	42.0
β (mJ/molK ⁴)	0.21	0.19	0.25	0.25
$\beta - y/3 \cdot \beta_{\text{Ru}}$ (mJ/molK ⁴)	0.18	0.15	0.21	0.20
$\Delta C(T_c)/\gamma T_c$	1.42	1.64	1.54	1.57
$N(E_F)$ (1/eV/u.c/spin)	7.82	7.64	8.33	8.90
λ	0.64	0.63	0.66	0.66
$N(E_F)/(1 + \lambda)$ (1/eV/u.c/spin)	4.78	4.68	5.03	5.36